

Revealing Mechanism and Origin of Reactivity of Au(I)-Catalyzed Functionalized Indenone Formation of Cyclic and Acyclic Acetals of Alkynylaldehydes

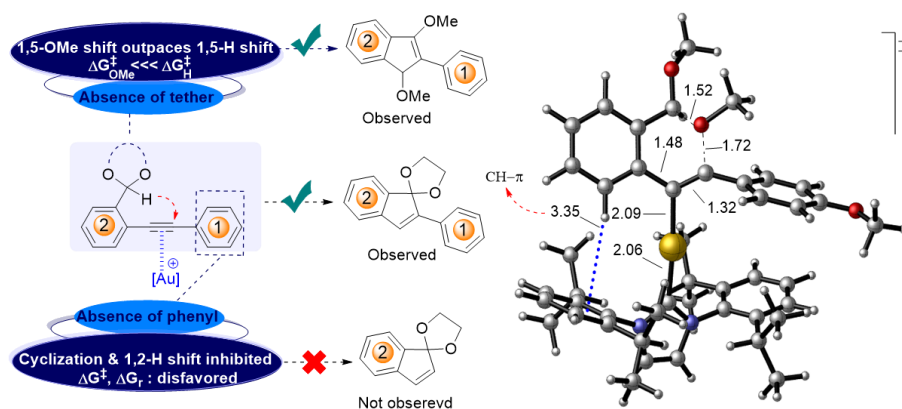
Aqeel A. Hussein^{1‡*} and Hafiz S. Ali^{2‡}

¹ College of Dentistry, University of Al-Ameed, Karbala PO Box 198, Iraq.

² Department of Chemistry and Manchester Institute of Biotechnology, The University of Manchester, 131 Princess Street, Manchester M1 7DN, UK.

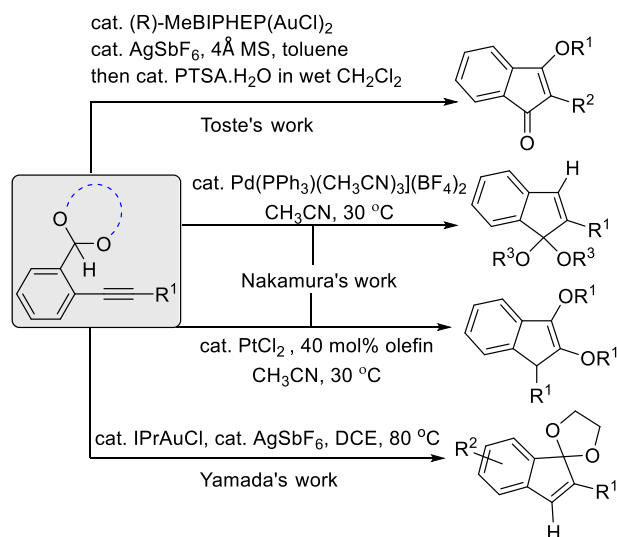
Abstract

Density functional theory exploited with the (SMD)-B3LYP-D3/def2-TZVP//B3LYP/6-31G(d),LANL2DZ level of theory is presented to offer mechanistic insights and explications of experimentally intriguing observations in the Au(I)-catalyzed cyclization of cyclic and acyclic acetals of alkynylaldehydes that lead to indenone formation. The reactivity of catalytic cycles with and without methoxy migration is computationally defined when alkyne terminus is phenylated in addition to the unreactive cycle when alkyne terminus is not phenylated. The reaction mechanism of indenone formation proceeds first with coordination of Au(I) to alkyne to initiate the reaction with 1,5-H shift as a rate-determining step and the fastest 1,5-H shift is achieved when one phenyl ring carries electron-donating group and the other one is substituted with electron-withdrawing group. The absence of tethered acetal unit considerably outpaces any 1,5-H shift and instead activates 1,5-methoxy migration, giving methoxy-migrated indenone, with the step of 1,2-OMe shift is a rate-limiting step during reaction pathway. Following 1,5-H shift the cyclization and 1,2-H shift are kinetically and thermodynamically feasible, which are followed by elimination to persist the iterative cycle, but the reactivity of both steps is highly affected by the existence of phenyl group on alkyne terminus. The unreactivity of alkyne terminus being not beared a phenyl ring is due to that the cyclization is thermodynamically disfavorable, subsequently deactivating the 1,2-H shift kinetically and thermodynamically.



Introduction

Indenones represent common motifs of carbocycles with a prime of importance in many structurally complex bioactive compounds or natural products.¹ Several synthetic methods of indenone have been shown to give moderate selectivities and yields using gold catalysis,^{2,3} iodine-mediated strategy,⁴ and organolithium reagents.⁵ Therefore, advancing a catalytically efficient approach has motivated and attracted many synthetic groups by which a metal-catalyzed cyclization was a premier route being targeted. For example, using the Au-catalyzed strategy to construct carbocycles, Hashmi *et al.* developed an intermolecular C(sp³)-C(sp²) bond formation in benzylic acetal compounds,⁶ Gagosz *et al.* utilized the intramolecular hydride shift from benzyl ethers to alkynes and allenes,⁷ and Toste and co-workers focused on cyclization of 2-alkynylbenzaldehyde dialkyl acetals (Scheme 1).⁸ Furthermore, Nakamura and Yamamoto and co-workers discovered the Pt- and Pd-catalyzed cyclization of 2-alkynylbenzaldehyde dialkyl acetals to achieve carbocycles (Scheme 1).⁹ Furthermore, hydride shift methodology have been also used and well-recognized in literatures for carbocycle synthesis.^{7,10} Recently, Yamada and co-workers have evolved a highly selective and yielding Au-catalyzed synthesis of functionalized indenone derivatives through cyclization of 2-alkynylaldehyde cyclic or tethered acetals that involves 1,5-hydride shifts promoted by the acetal group (Figure 1-a).¹¹ The functionalized indenones were achieved in high a yield and selectivity when the aldehyde group was protected with a tethered acetal unit. However, in the absence of tether a methoxy-migrated product was obtained (Figure 1-a). This in fact stimulates inquiries and further examinations to comprehend the factors that control the origin of reactivity.



Scheme 1. Transformation of 2-Alkynylaldehyde (a)cyclic acetal into indenone derivatives.

The mechanism reaction of indenone formation shown in Figure 1-b indicated that the gold catalyst is first coordinated to alkyne to give vinyl gold intermediate that subsequently undergoes 1,5-shift and then cyclization of the oxonium cation to give a cyclized Au(I)-carbene intermediate, and finally a 1,2-H shift to afford the indenone derivatives **2** (**Figure 1-b**, left). Importantly, the migration mechanism of an acetal unit (or methoxy group) is tolerable when acetal group is untethered and proceeds in a similar mechanistic pathway to that of 1,5-H initiated pathway (**Figure 1-b**, right). It seems that the tether impedes the migration and activates the benzylic C–H bond to promote the 1,5-H shift and deactivates the 1,5-methoxy migration.¹¹ Therefore, understanding this transformation is highly sound regarding the detailed description of reaction mechanism and the origin of reactivity for this catalysis. We were then interested in several questions coincide with this transformation to be studied and performed through computational approaches of DFT quantum mechanics to evaluate the feasibility of the proposed reactivity of Au(I)-catalyzed cyclization to provide an insight into the nature of cyclization if it is stepwise or concerted C–H insertion (**Figure 1-c**). Furthermore, competition between 1,5-H and 1,4-H shift, comparison between the tethered- and untethered-involved acetal unit migration pathway, the effect of electronic groups on the rate-determining step of the reaction pathway, and the structures of the 2-alkynylaldehyde cyclic acetals that facilitate a comparison of rate effects on reactivity will be rationalized computationally (**Figure 1-c**).¹²

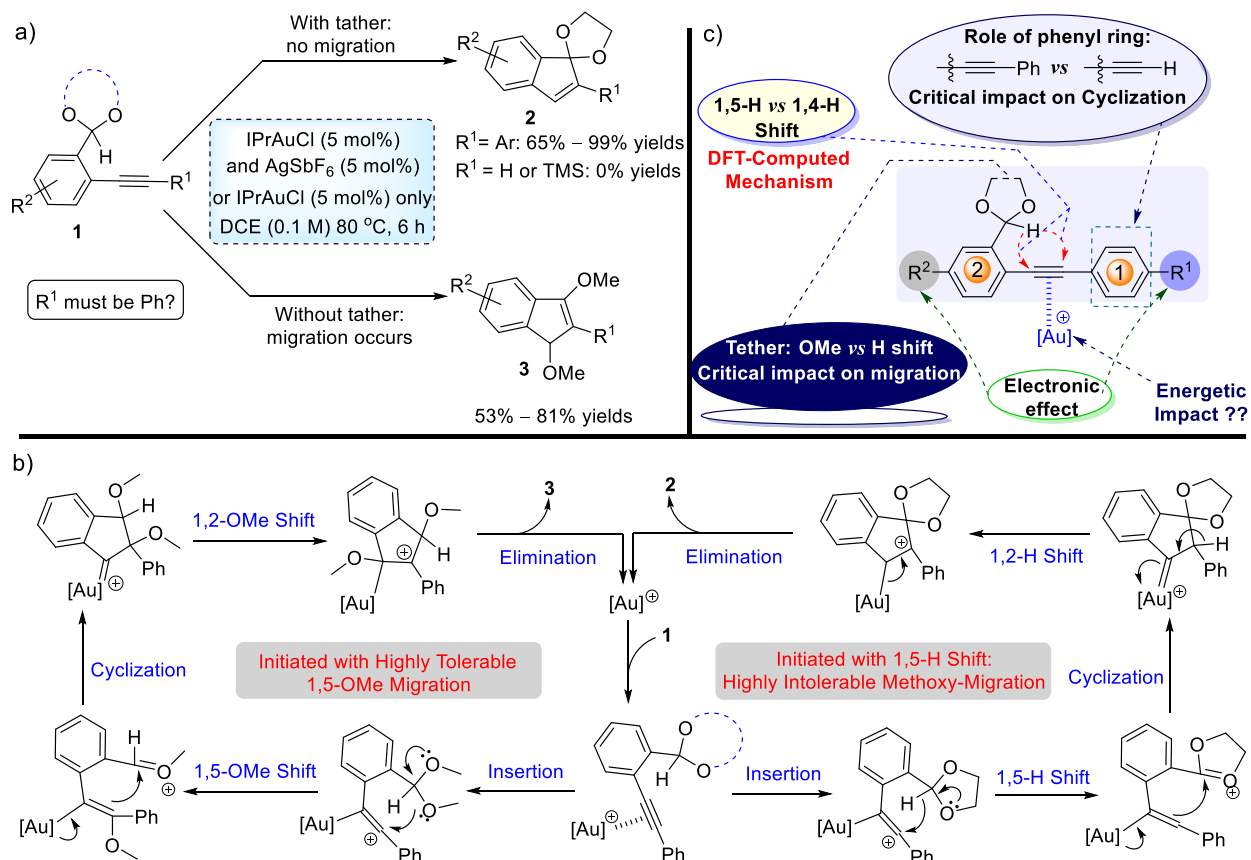


Figure 1. (a) Au-catalyzed cyclization of 2-alkynylaldehyde cyclic or acyclic acetals for the synthesis of functionalized indenone derivatives. (b) Summary of the factors interrogated in this study. (c) Mechanism of the Au-catalyzed cyclization of 2-alkynylaldehyde tethered acetals for the synthesis of functionalized indenone derivatives.

Results and Discussion

To explore the mechanism and factors that control reactivity of this synthetically useful transformation, our DFT interrogations are divided to three parts: (1) the reaction mechanism of the Au-catalyzed cyclization of 2-alkynylaldehyde tethered acetals for the indenone synthesis; (2) the substituents effect involve: (a) the electronic effect, (b) the origin of reactivity crystallized by absence of phenyl ring on alkyne terminus, and (c) justification of the origin of methoxy migration when untethered acetal unit is presents. Based on experimental conditions shown in Figure 1-a, the presence of IPrAuCl/AgSbF₆ will lead to salt metathesis or double displacement to give IPrAuSbF₆ and AgCl to supply the reaction with IPrAu⁺ as a more likely “naked” counterion due to its counter-anion (SbF₆[−]) is large enough to be far away from IPrAu⁺. In this regard, using IPrAuSbF₆ will also give IPrAu⁺ in the reaction. Previous studies show that the anionic SbF₆[−] found to have a little impact on the reactions¹³ and thus, the cationic IPrAu⁺ is employed as the active

catalyst in this study. All our DFT simulations were conducted with the B3LYP-D3/def2-TZVP level of theory in SMD solvation model using dichloroethane (DCE) as a representative solvent based on gas phase optimization performed with the B3LYP/6-31G(d), LANL2DZ level of theory (see computational details).

Mechanism of tethered substrate. We began our mechanistic incursions with the mechanism of Au-catalyzed cyclization of tethered acetal 2-alkynylaldehyde (**1a**) to form 2-(4-methoxyphenyl)spiro[indene-1,2'-[1,3]dioxolane] (**2a**) (Figure 2). The reaction overall composes of five important steps; Au insertion, 1,5-shift, cyclization, 1,2-shift and elimination. A superior consideration for the effect of catalyst on reaction, we have compared the results of Au-catalyzed and uncatalyzed pathways directly and shown in Figure 2. Initially, insertion of catalyst to the alkyne (**1a**) is calculated to be an exergonic step of 14.7 kcal/mol to give intermediate **Int1a** with Au—C bond distances of 2.24 and 2.45 Å where the charge is on carbon of alkyne stabilized by the neighbored *p*-methoxy phenyl ring. Following insertion, the intermediate **Int1a** undergoes 1,5-H shift via TS **TS1a**, where the transferable hydrogen atom is closer to the acetal (C—H = 1.27 Å) from alkyne (C—H = 1.40 Å), with barrier of 17.5 kcal/mol leading to **Int2a** as a slightly thermodynamically favored step ($\Delta G_r = -3.1$ kcal/mol). In comparison with the uncatalyzed 1,5-H shift, the barrier is substantially high ($\Delta G^\ddagger = 45.6$ kcal/mol, **TS1'**), and the cyclization and 1,2-H shift are highly disfavored too in accordance with experimental conditions (Figure 2). Following the formation of **Int2a**, the cyclization proceeds with a barrier of 16.8 kcal/mol via TS **TS2a** to pass the transient distance of 2.12 Å to give the cyclized intermediate **Int3a** as a nearly thermoneutral step ($\Delta G_r = -1.0$ kcal/mol). After cyclization the charge moves back on the Au by which the Au—C shortens to 2.01 Å whereas it was 2.08 Å before cyclization. Now, if the intermediate **Int3a** is thermodynamically unstable, the final transition before releasing the final product is presumably a rate-determining step (RDS). The 1,2-H shift overcomes **TS3a** with a barrier of 17.0 kcal/mol to give intermediate **Int4a** as a thermodynamically favored ($\Delta G_r = -15.4$ kcal/mol) and the charge is situated on the tertiary carbon and settled by phenyl ring. The cyclization ($k = 5.2 \times 10^2 \text{ s}^{-1}$) is approximately twice faster than 1,2-H shift ($k = 2.9 \times 10^2 \text{ s}^{-1}$) and, therefore, the latter step is a RDS. Comparison between the three transient steps (**TS1a**, **TS2a** and **TS3a**), the 1,5-H shift is a RDS for the indenone formation. Finally, to persist the iterative cycle of Au-catalyzed indenone pathway, the elimination is calculated to be thermoneutral ($\Delta G_r = -2.0$ kcal/mol) to release **2a** and reform **Int1a**, where the release of **2a** is thermodynamically driven by the reformation of **Int1a**.

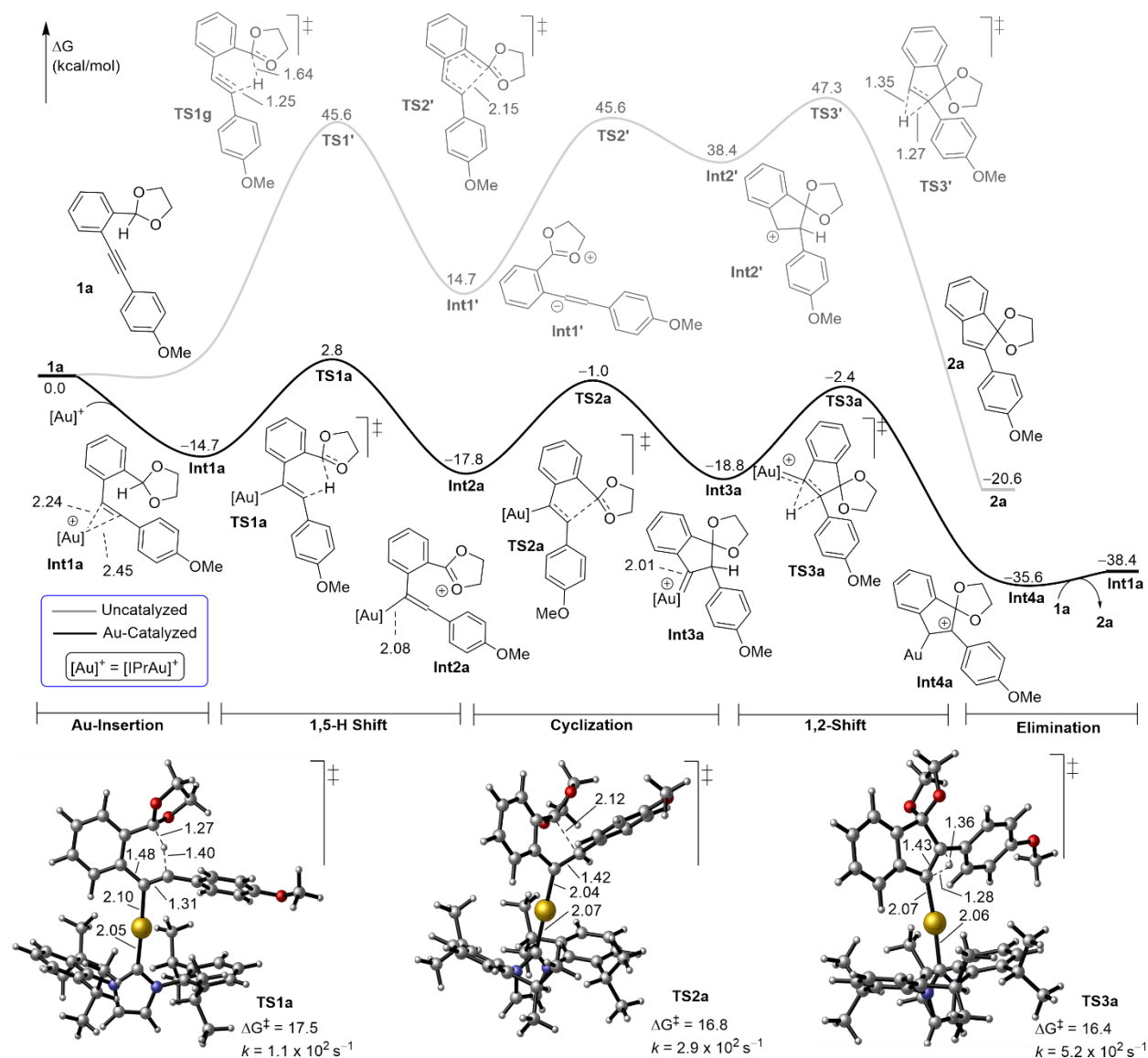


Figure 2. Free energy profile for Au-catalyzed and uncatalyzed cyclization pathway of 2-alkynylaldehyde tethered acetals **1a** for the synthesis of indenone **2a**. The optimized TSs for the Au-catalyzed pathway are only shown here. Bond lengths are in Å. Free energies and rate constants are calculated at 353.15 K.

Our calculations above support the stepwise pathway of indenone **2a** formation but we have considered the concerted mechanism by which a 1,4-H shift and cyclization occur at the same time.^{10c} Our DFT investigations did not signalize any concerted TS and, so, it was totally excluded. However, we considered the stepwise mechanism starting with 1,4-H shift followed by cyclization. Figure 3 shows competition pathways initiated at 1,5-H and 1,4-H shifts. The results elucidate that the 1,4-H shift is ruled out due to a high barrier of 26.6 kcal/mol ($k = 2.5 \times 10^{-4} \text{ s}^{-1}$) required whereas the 1,5-H shift needs 17.5 kcal/mol ($k =$

$1.1 \times 10^2 \text{ s}^{-1}$) by which the earlier pathway is slower by 4.4×10^5 times although cyclization ($\Delta G^\ddagger = 8.3$ kcal/mol, $k = 5.4 \times 10^7 \text{ s}^{-1}$) from 1,4-H shift-initiated pathway is calculated to be substantially faster than cyclization ($\Delta G^\ddagger = 16.8$ kcal/mol, $k = 2.9 \times 10^2 \text{ s}^{-1}$) initiated from 1,5-H shift.

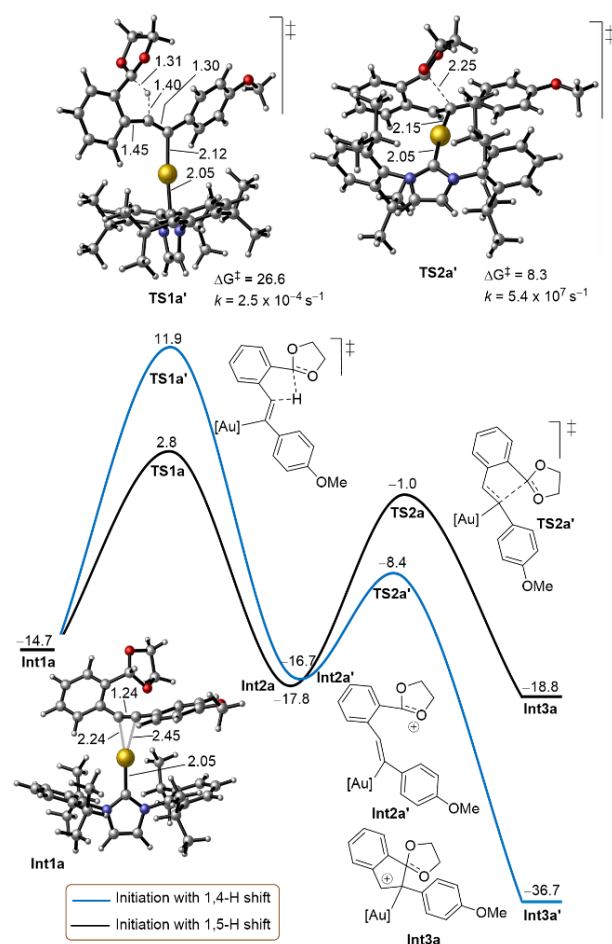


Figure 3. Free energy profile for Au-catalyzed cyclization pathway of **1a**, showing competition between 1,4-H and 1,5-H shift. The optimized TSs for the Au-catalyzed pathway are only shown. Structures of 1,5-H shift initiation pathway is shown in Figure 2. Bond lengths are in Å. Free energies and rate constants are calculated at 353.15 K

Electronic effect on 1,5-H shift. We have next carried out DFT simulations to understand the effect of electron-withdrawing (EWG) and electron-donating (EDG) groups on the 1,5-H shift step represented by both aromatic rings (Figure 4). Substituents on aromatic rings 1 and 2 encompass different impacts on rate constant of 1,5-H shifts (Figure 4-a). The phenyl ring 1 substituted with donating groups show lower barriers than those with withdrawing groups whereas the unsubstituted one has a moderate barrier height. In comparison to **1a** ($\Delta G^\ddagger = 17.5$ kcal/mol, $k = 1.1 \times 10^2 \text{ s}^{-1}$, **TS1a**), the rate constant drops by one and half times when methoxy group is replaced with $R^1 = \text{CO}_2\text{Me}$ **Intc** ($\Delta G^\ddagger = 17.8$ kcal/mol, $k = 7.1 \times 10^1 \text{ s}^{-1}$, **TS1c**)

due to barrier difference of $\Delta\Delta G^\ddagger = 0.3$ kcal/mol. When $R^1 = H$, **In1b**, the 1,5-H shift displays higher barrier via **TS1b** than *p*-OMe group via **TS1a** by $\Delta\Delta G^\ddagger = 1.0$ kcal/mol, slower by more than 4 times than **TS1a** and nearly 3 times than **TS1c**. When the other phenyl ring on **1a** was substituted with methoxy group, **Int1e**, R^1 and $R^2 = OMe$, the barrier increases to 18.7 kcal/mol via **TS1e** with the impact on rate constant being slower by more than 5 times than **TS1a**. Interestingly, the presence $R^2 = NO_2$ and $R^1 = OMe$, **In1d**, drop the barrier by 1.5 kcal/mol compared to **Int1a** which relatively results in a rate constants being nine times faster than **TS1a**. This indicates that when one of the phenyl rings is EDG and other one is EWG, the rate constants increase by 46 times. Analysis of the noncovalent interactions (NCI) along TSs **TS1a-e** were also performed (see computational details) and appeared in Figure 4-b. Although the presence of many functional groups, especially the aromatic rings on the substrates **1a-e** and NHC ligand, we have not recognized a clear interaction. Although the isosurfaces of NCI interactions were processed with an isovalue of 0.7, a weak CH- π stacking interaction between phenyl 1 on substrate and phenyl of NHC part has noticed. The CH- π interaction between phenyl 2 and the phenyl of NHC is absent although both rings comprise a nearly T-shaped form. What is recognizable from NCI calculations is the main interactions between the four isopropyl group on aromatic rings of NHC ligand and gold atom like a four-membered cage. Frontier orbital analysis of the five TSs **TS1a-e** are shown in Figure 4-c, especially the spatial plots associated with the bonding orbitals, namely highest occupied molecular orbitals (HOMOs). An overall delocalization for the orbitals is indicated over the whole TS from phenyl ring 1 to 2.

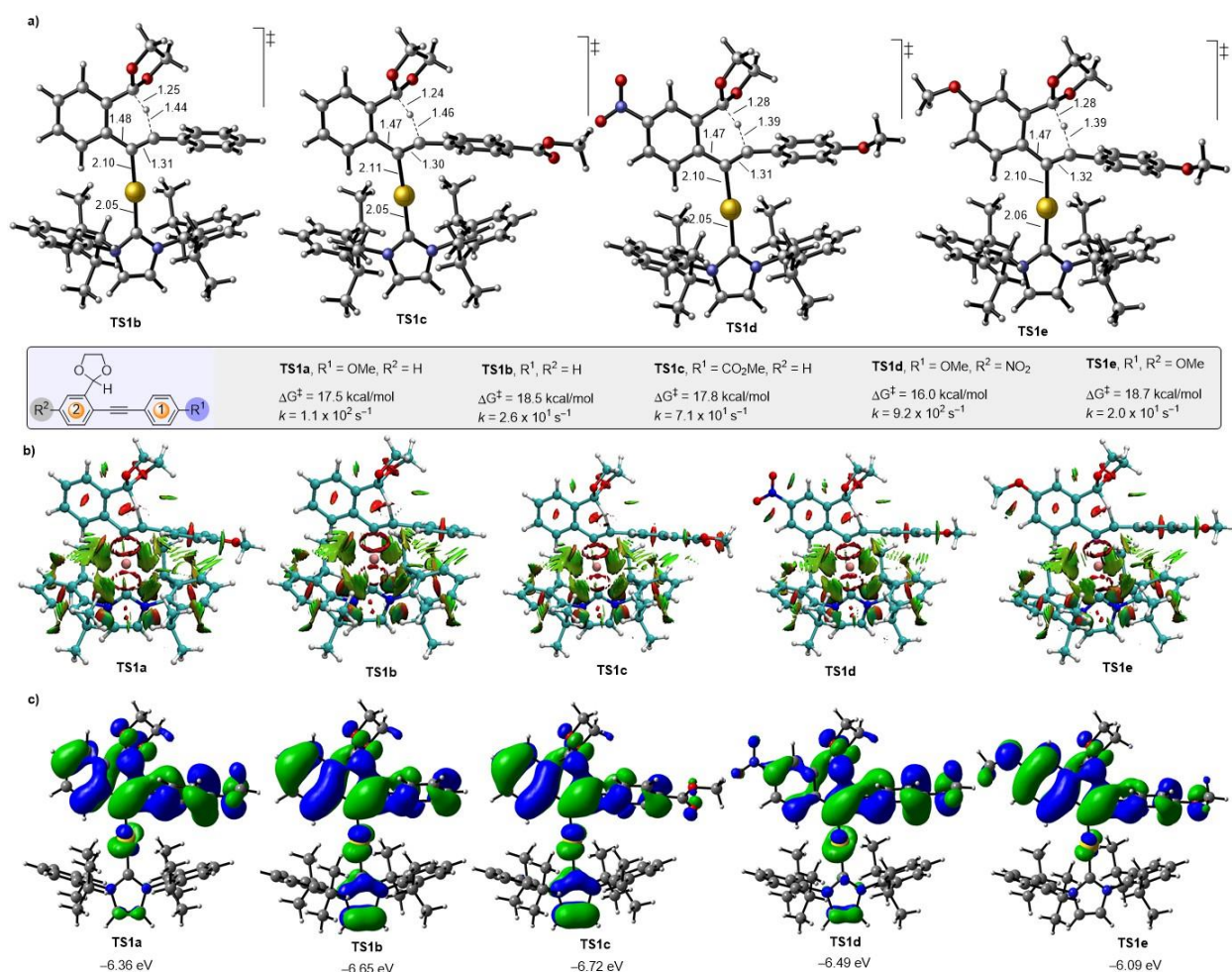


Figure 4. (a) Optimized TSs for the 1,5-H shift step with different substituents of R^1 and R^2 for **TS1a-e**. (b) NCI isosurfaces (isovalued at 0.7) associated with the TSs **TS1a-e**, where NCI interactions are shown in green. (c) Spatial plots of the bonding orbitals associated with the TSs **TS1a-e**. Bond lengths are in Å. Free energies and rate constants are calculated at 353.15 K

Reactivity of unsubstituted alkyne terminus. Experimentally, when terminal alkyne was not beared a phenyl ring as shown in alkyne **1f**, its indenone product was not formed.¹¹ Following the same protocol shown above, our interrogations referred to that this substrate can participate in 1,4-H and 1,5-H shift initiations with the 1,5-H shift being relatively faster (see **TS1f** and **TS1f'**, Figure 5). On one hand, our calculations revealed that the 1,4-H shift is higher than 1,5-H shift by 1.0 kcal/mol via TS **TS1f'** (Figure 5, right). This evidence that 1,4-H shift is relatively inaccessible when terminal alkyne is not substituted with phenyl ring. Interestingly, **TS1f'** shows a T-shaped CH- π stacking interaction (Figure 6-a) between aromatic rings of substrate and NHC ligand at 3.11 Å. Indeed, this interaction participates to some extent

in lowering the barrier plus the stabilization arrived from Au atom that makes the 1,4-H to be more stabilized when compared to **TS1a**.

On the other hand, the calculated barrier for the 1,5-H shift via TS **TS1f** ($\Delta G^\ddagger = 17.4$ kcal/mol, Figure 5, left) is in line with that calculated for the one substituted with *p*-OMe phenyl **1a** (Figure 2). This 1,5-H shift involves a T-shaped CH- π stacking interaction like **TS1f** but at longer distance of 3.38 Å (see Figure 6-a). Although the cyclization barrier of intermediate **Int2f** through TS **TS2f** is faster, $\Delta G^\ddagger = 15.3$ kcal/mol, than cyclization in **1a**, the corresponding intermediate **Int3f** is unlikely thermodynamically endergonic ($\Delta G_r = 14.7$ kcal/mol). Due to disfavored cyclization, the 1,2-H shift will be disfavored too. The 1,2-H shift requires high barrier via **TS3f** of $\Delta G^\ddagger = 23.9$ kcal/mol ($k = 1.2 \times 10^{-2} \text{ s}^{-1}$) as an endergonic step ($\Delta G_r = 8.9$ kcal/mol). This increased barrier and undesirable thermodynamics would substantially impede the formation of the correspondent indenone. Therefore, initiation with 1,5-H shift leads to cyclization to be thermodynamically unlikely and 1,2-H shift to be very slow and, therefore, the correspondent indenone will be unreachable.

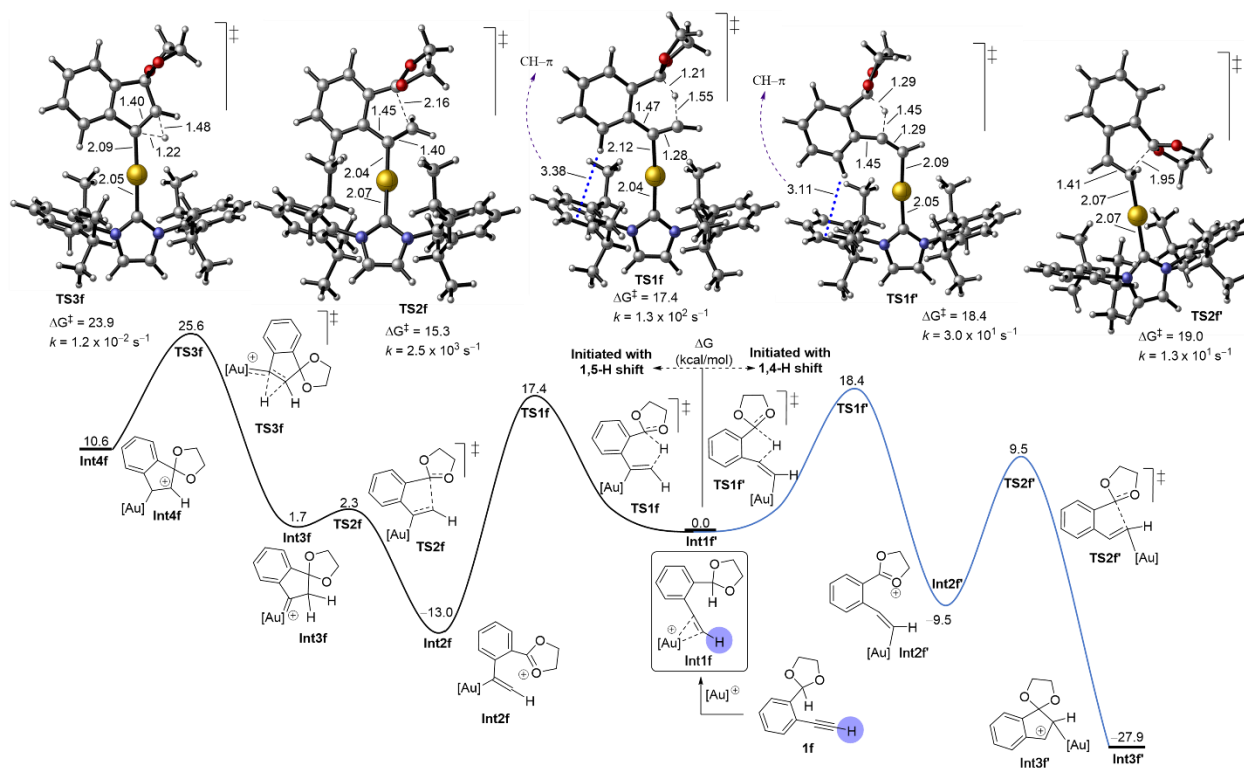


Figure 5. Free energy profile for Au-catalyzed cyclization of unsuccessful substrates **1f** showing reaction initiated from both 1,5-H (left) and 1,4-H (right) shifts when the phenyl group is absent on alkyne terminus. Bond lengths are in Å. Free energies and rate constants are calculated at 353.15 K

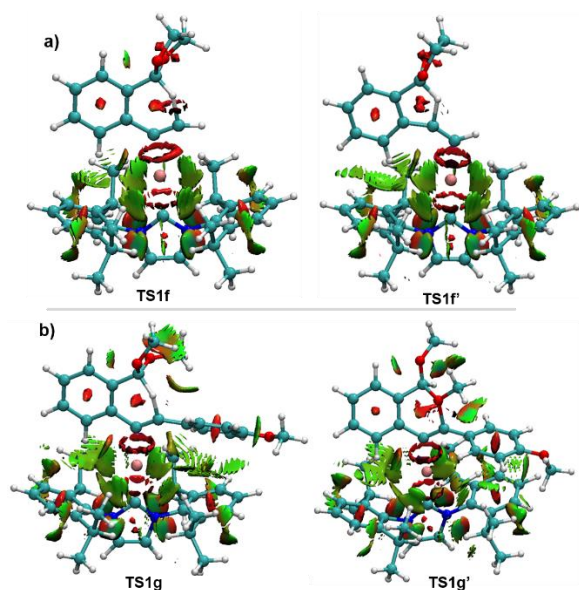


Figure 6. Plots of NCI isosurfaces (isovalue at 0.7): (a) **TS1f** and **TS1f'** and (b) **TS1g** and **TS1g'**.

Effect of tether (cyclic vs acyclic acetal group). One important experimental observation noticed from the results of Yamada and co-workers is the formation of methoxy-migrated product when aldehyde group was not protected with a cyclic acetal unit. In principle, the absence of tethered acetal unit stimulates two possible initiations starting from Au-inserted intermediate **Int1g**; either initiation with conventional 1,5-H shift or 1,5-methoxy migration (see Figure 1 and Figure 7). First, we performed DFT simulation on 1,5-H initiated pathway to examine the tether effect on energetic pathway for indenone formation (Figure 7, left). The barrier of 1,5-H shift step has increased from 17.5 kcal/mol in **TS1a** (Figure 2) to 22.1 kcal/mol in **TS1g** (Figure 7, left). The effect on cyclization and 1,2-H shift is changed when tethered bond is absent. The cyclization overcomes a lower barrier of 7.3 kcal/mol in **TS2g**, as a nearly thermoneutral step, compared to 16.8 kcal/mol in **TS2a** (Figure 2). The 1,2-H shift becomes slower with a barrier of 19.4 kcal/mol via **TS3g** compared to 16.4 kcal/mol in **TS3a**.

Second, the methoxy migration proceeds with predominantly lower energetic pathway (Figure 7, right). The methoxy migration TS **TS1g'** overcomes a barrier of 17.4 kcal/mol, being 4.7 kcal/mol under 1,5-H shift with the product of methoxy-migrated pathway, **Int2g'**, becomes endergonic ($\Delta G_r = 6.2$ kcal/mol). The favorability of methoxy migration over 1,5-H shift explain the importance of tether in promoting the 1,5-H shift and prevent migration. The cyclization is very fast step of only 8.5 kcal/mol ($k = 4.0 \times 10^7 \text{ s}^{-1}$, **TS2g'**) to give the cyclized product **Int3g'** as an approximately thermoneutral step ($\Delta G_r = -0.5$ kcal/mol). The latter, **Int3g'**, requires 16.0 kcal/mol via **TS3g'** to process the 1,2-methoxy shift to release **Int4g'** as an exergonic step of $\Delta G_r = -36.8$ kcal/mol. It is important to see here that the methoxy-migrated pathway shows that 1,2-methoxy shift to be a rate-determining step whereas in the tethered acetal pathway (see

Figure 2) the 1,5-H shift is RDS. Overall, the current results explain the mechanism of the observed experimental methoxy migrated product as the favored product (see Figure 1-a).

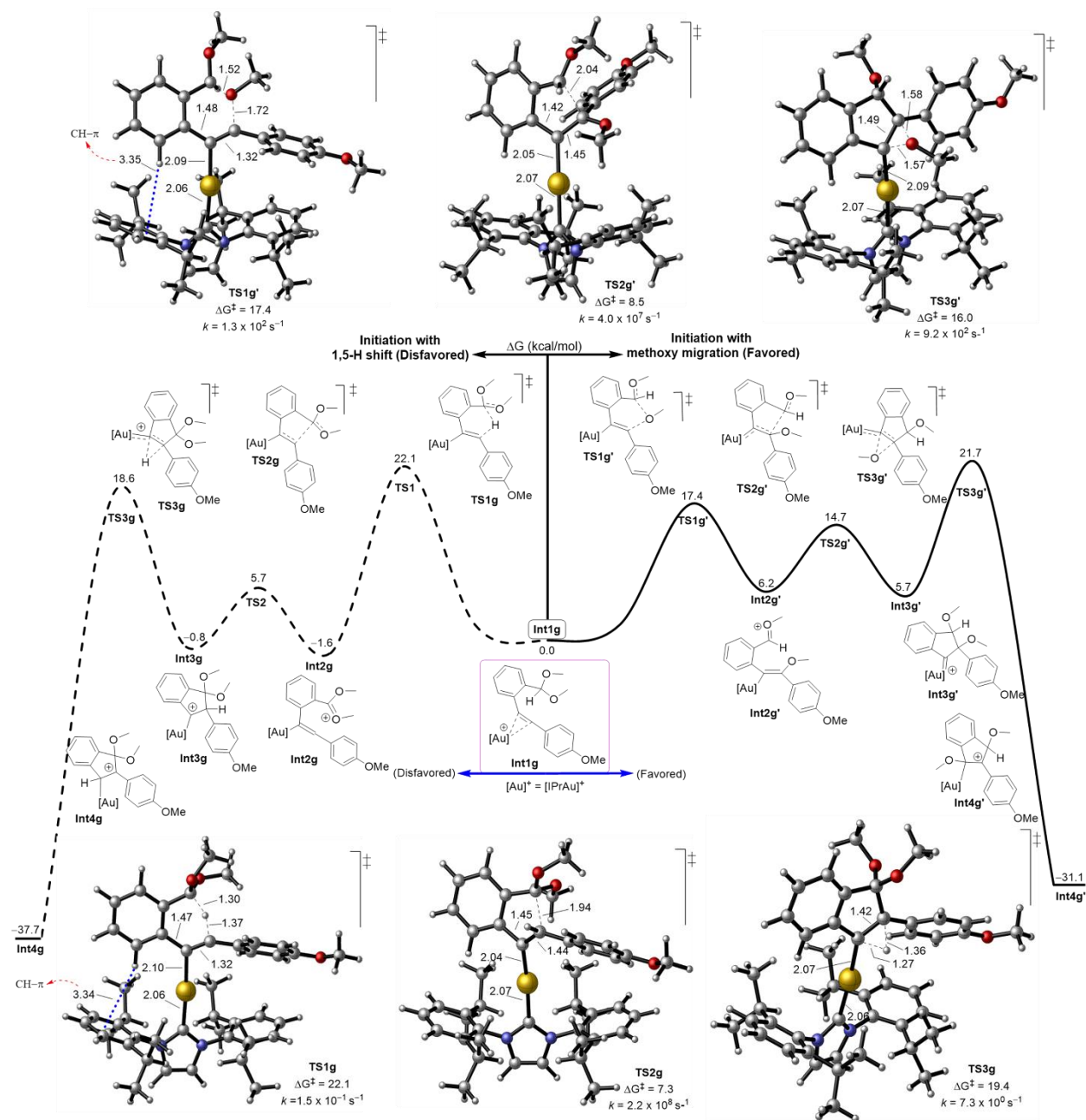


Figure 7. Free energy profile of Au-catalyzed cyclization of untethered acetal substrate **1g** initiated at the 1,5-H shift (left) and the methoxy migration (right). Only TSs are shown. Bond lengths are in Å. Free energies and rate constants are calculated at 353.15 K.

Conclusions

We have exploited DFT calculations with the (SMD)-B3LYP-D3/def2-TZVP//B3LYP/6-31G(d),LANL2DZ level of theory to provide mechanistic insights into the Au-catalyzed cyclization of cyclic and acyclic acetals of alkynylaldehydes that lead to indenone formation. Our findings are consistent with experimental observations. We have clarified two catalytic cycles leading to the indenone formation with and without methoxy migration based on the structure of applied substrate in addition to the unreactive cycle for the phenyl-absent alkyne terminus. The feasibility of the proposed reactivity was confirmed and proceeded through five important steps: (1) Au(I) insertion as a thermodynamically sink step, (2) 1,5-H shift as an RDS, cyclization, and 1,2-H shift as kinetically and thermodynamically convenient steps and (3) elimination through exchangeable insertion with another alkyne to persist the iterative cycle. DFT simulation revealed that following Au-insertion the 1,5-H shift is highly favored over 1,4-H shift although the barrier of 1,4-H initiation decreases when alkyne terminus was not beared a phenyl group. Effect of substituents concerning EDGs and EWGs on the 1,5-H shift were considered on both phenyl rings of alkynlaldehyde and showed different rates with the highest rate achieved when a substrate carries EDG on one phenyl ring and EWG on the other phenyl ring. Two critical intriguing phenomenons that limit the productivity of the indenone formation are the effect of tethered acetal unit and the substitution on alkyne terminus. When the alkyne terminus was not beared a phenyl ring, the corresponding indenone product was not observed due to that the cyclization was found to be thermodynamically disfavorable which consequently leads to deactivate the 1,2-H shift kinetically and thermodynamically. Interrogating the pathways of tethered- and untethered-involved acetal unit revealed that the untethered acetal substrate mainly starts with 1,5-methoxy migration as a kinetic product and considerably outpaces any 1,5-H shift, asserting the experimentally observed methoxy-migrated indenone product and explaining the role of tether in promoting the 1,5-H shift over methoxy shift. Comparison between the tethered- and untethered-involved acetal unit pathways defined the 1,5-H shift being RDS when acetal unit is tethered whereas the 1,2-OMe shift becomes RDS when acetal unit is untethered.

Computational details

All quantum calculations were performed using Gaussian 09¹⁴ with the B3LYP density functional theory method (DFT).¹⁵ All geometry optimizations were performed with the B3LYP/6-31G(d),LANL2DZ level of theory by which the basis sets 6-31G(d) basis was set for all atoms except Au whereas an effective core potential basis set LANL2DZ was used for Au atom.¹⁶ All minima intermediates were verified by the absence of negative eigenvalues in the vibrational frequency analysis while all the transition state structures were found using the Berny algorithm,¹⁷ and verified by vibrational analysis through animating the negative eigenvector coordinate. In order to correct the energetics and account the effect of solvent, single-point

energies of the optimized geometries were evaluated with the same DFT functional (B3LYP) but with Ahlrichs basis set def2-TZVP¹⁸ and the dispersion corrections (D3) developed by Grimme¹⁹ was added to calculations in dichloroethane (DCE) as a representative solvent medium with universal solvation model based on density (IEFPCM-SMD).²⁰ To obtain the free energies at 353.15 K and 1 atm, the thermal corrections evaluated from the unscaled vibrational frequencies at the B3LYP/6-31G(d),LANL2DZ level of theory were then added to the electronic energies calculated from the B3LYP-D3/def2-TZVP level of DFT. Intrinsic reaction coordinate (IRC) calculations were performed for the identified transition states to confirm the reaction path proceeding in both directions (reactant and product), in which the Hessian was recomputed every 3 predictor steps with a step size along the reaction path of 0.05 Bohr.²¹ The optimized structures indicated and shown in this study are illustrated using CYLview program.²² To account the presence of non-covalent interactions, Reduced Density Gradient (RDG) analysis²³ is performed using the Multiwfn program²⁴ and visualized by Visual molecular dynamics (VMD).²⁵

ASSOCIATED CONTENT

Supporting Information

The Supporting Information is available free of charge on the ACS Publications website.

Absolute energies and cartesian coordinates (PDF)

AUTHOR INFORMATION

Corresponding Author

Aqeel A. Hussein - College of Dentistry, University of Al-Ameed, Karbala PO Box 198, Iraq;
orcid.org/0000-0002-9259-9609; Email: aqeel_alaa85@yahoo.com

Authors

Hafiz S. Ali - Department of Chemistry and Manchester Institute of Biotechnology, The University of Manchester, 131 Princess Street, Manchester M1 7DN, UK.; orcid.org/0000-0001-5770-5376

Author Contributions

‡These authors contributed equally.

Notes

The authors declare no competing financial interest.

Acknowledgements

The authors acknowledge the computational resources from computational shared facility (CSF) supported by the University of Manchester and the iridis4 supercomputers supported by the University of Southampton. Many thanks to Prof. Sami Lakhdar for his valuable proofreading. A.A.H. highly acknowledges the University of Southampton/School of Chemistry for providing the visitor-status research position (2717441/EB00-VISIT), especially Prof. Richard C. D. Brown.

References

- 1- For selected bioactive indenone-involved compounds see: (a) Liu, F.; Dong, Z.; Wang, J.; Dong, G. Palladium/Norbornene-Catalyzed Indenone Synthesis from Simple Aryl Iodides: Concise Syntheses of Pauciflorol F and Acredinone A. *Angew. Chem., Int. Ed.* **2019**, *58*, 2144–2148. (b) Yeon, J.-T.; Kim, H.; Kim, K.-J.; Lee, J.; Won, D. H.; Nam, S.-J.; Kim, S. H.; Kang, H.; Son, Y.-J. Acredinone C and the Effect of Acredinones on Osteoclastogenic and Osteoblastogenic Activity. *J. Nat. Prod.* **2016**, *79*, 1730–1736. (c) Morrell, A.; Placzek, M.; Parmley, S.; Grella, B.; Antony, S.; Pommier, Y.; Cushman, M. Optimization of the Indenone Ring of Indenoisoquinoline Topoisomerase I Inhibitors. *J. Med. Chem.* **2007**, *50*, 4388–4404. (d) Ahn, J. H.; Shin, M. S.; Jung, S. H.; Kang, S. K.; Kim, K. R.; Rhee, S. D.; Jung, W. H.; Yang, S. D.; Kim, S. J.; Woo, J. R.; Lee, J. H.; Cheon, H. G.; Kim, S. S. Indenone Derivatives: A Novel Template for Peroxisome Proliferator-Activated Receptor γ (PPAR γ) Agonists. *J. Med. Chem.* **2006**, *49*, 4781–4784. For selected natural products see: (e) Liu, Z.; Qiu, P.; Li, J.; Chen, G.; Chen, Y.; Liu, H.; She, Z. Anti-inflammatory polyketides from the mangrove-derived fungus *Ascomycota* sp. SK2YWS-L. *Tetrahedron* **2018**, *74*, 746–751. (f) Fathy, H. M.; Aboushoer, M. I. A New Indenone from *Echiochilon f. ruticosum*, a Potential BACE1 and Acetylcholinesterase (AChE) Inhibitor. *Der Pharma Chemica* **2017**, *9*, 100–103. (g) Wiechmann, K.;

Müller, H.; Huch, V.; Hartmann, D.; Werz, O.; Jauch, J. Synthesis and biological evaluation of novel myrtucommulones and structural analogues that target mPGES-1 and 5-lipoxygenase. *Eur. J. Med. Chem.* **2015**, *101*, 133–149.

- 2- For general gold catalysis approaches see: (a) Sekine, K.; Schulmeister, J.; Paulus, F.; Goetz, K. P.; Rominger, F.; Rudolph, M.; Zaumseil, J.; Hashmi, A. S. K. Gold-Catalyzed Facile Synthesis and Crystal Structures of Benzene-/Naphthalene-Based Bis-pentalenes as Organic Semiconductors. *Chem. - Eur. J.* **2019**, *25*, 216–220. (b) Pflasterer, D.; Hashmi, A. S. K. Gold catalysis in total synthesis – recent achievements. *Chem. Soc. Rev.* **2016**, *45*, 1331–1367. (c) Li, Y.; Li, W.; Zhang, J. Gold-Catalyzed Enantioselective Annulations. *Chem. - Eur. J.* **2017**, *23*, 467–512. (d) Dorel, R.; Echavarren, A. E. Gold(I)-Catalyzed Activation of Alkynes for the Construction of Molecular Complexity. *Chem. Rev.* **2015**, *115*, 9028–9072. (e) Ohno, H. Gold-Catalyzed Cascade Reactions of Alkynes for Construction of Polycyclic Compounds. *Isr. J. Chem.* **2013**, *53*, 869–882. (f) Obradors, C.; Echavarren, A. M. Intriguing mechanistic labyrinths in gold(I) catalysis. *Chem. Commun.* **2014**, *50*, 16–28. (g) Bandini, M. Gold-catalyzed decorations of arenes and heteroarenes with C–C multiple bonds. *Chem. Soc. Rev.* **2011**, *40*, 1358–1367. (h) Hashmi, A. S. K. Homogeneous Gold Catalysis Beyond Assumptions and Proposals—Characterized Intermediates. *Angew. Chem. Int. Ed.* **2010**, *49*, 5232–5241. (i) Fürstner, A. Gold and platinum catalysis—a convenient tool for generating molecular complexity. *Chem. Soc. Rev.* **2009**, *38*, 3208–3221. (j) Arcadi, A. Alternative Synthetic Methods through New Developments in Catalysis by Gold. *Chem. Rev.* **2008**, *108*, 3266–3325. (k) Shen, H. C. Recent advances in syntheses of carbocycles and heterocycles via homogeneous gold catalysis. Part 2: Cyclizations and cycloadditions. *Tetrahedron* **2008**, *64*, 7847–7870. (l) Gorin, D. J.; Toste, F. D. Relativistic effects in homogeneous gold catalysis. *Nature* **2007**, *446*, 395–403. (m) Hashmi, A. S. K.; Hutchings, G. J. Gold Catalysis. *Angew. Chem. Int. Ed.* **2006**, *45*, 7896–7936.
- 3- For selected gold catalysis methodologies see: (a) Yin, X.; Mato, M.; Echavarren, A. M. Gold(I)-Catalyzed Synthesis of Indenes and Cyclopentadienes: Access to (±)-Laurokamurene B and the Skeletons of the Cycloaurenones and Dysiherbols. *Angew. Chem. Int. Ed.* **2017**, *56*, 14591–14595. (b) Mokar, B. D.; Hupke, D. B.; Liu, R.-S. Gold-catalyzed Intermolecular Oxidations of 2-Ketonyl-1-ethynyl Benzenes with N-Hydroxyanilines to Yield 2-Aminoindenediones via Gold Carbene Intermediates. *Angew. Chem. Int. Ed.* **2016**, *55*, 11892–11896. (c) Chen, Y. Gold-Catalyzed Ammonium Acetate Assisted Cascade Cyclization of 2-Alkynylarylketones. *J. Org. Chem.* **2015**, *80*, 11360–11368. (d) For one example using an iodoalkyne via a gold vinylidene complex, see: Moran-Poladura, P.; Rubio, E.; González, J. M. Intramolecular C–H Activation through Gold(I)-Catalyzed Reaction of Iodoalkynes. *Angew. Chem. Int. Ed.* **2015**, *54*, 3052–3055.

- 4- Chuangsoongnern, P.; Surinrach, C.; Tummatorn, J.; Thongsornkleeb, C.; Ruchirawat, S. Iodine-Mediated Cyclization of ortho-Alkynylaryl Ketones for the Synthesis of Indenone Derivatives. *Eur. J. Org. Chem.* **2017**, 2017, 5102–5109.
- 5- Katsumoto, K.; Kitamura, C.; Kawase, T. An Indenone Synthesis Involving a New Aminotransfer Reaction and Its Application to Dibenzopentalene Synthesis. *Eur. J. Org. Chem.* **2011**, 2011, 4885–4891.
- 6- Yu, Y.; Yang, W.; Rominger, F.; Hashmi, A. S. K. In Situ Generation of Nucleophilic Allenes by the Gold-Catalyzed Rearrangement of Propargylic Esters for the Highly Diastereoselective Formation of Intermolecular C(sp³)–C(sp²) Bonds. *Angew. Chem., Int. Ed.* **2013**, 52, 7586–7589.
- 7- (a) Bolte, B.; Gagosz, F. Gold and Brønsted Acid Catalyzed Hydride Shift onto Allenes: Divergence in Product Selectivity. *J. Am. Chem. Soc.* **2011**, 133, 7696–7699. (b) Jurberg, I. D.; Odabachian, Y.; Gagosz, F. Hydroalkylation of Alkynyl Ethers via a Gold(I)-Catalyzed 1,5-Hydride Shift/Cyclization Sequence. *J. Am. Chem. Soc.* **2010**, 132, 3543–3552. (c) Bolte, B.; Odabachian, Y.; Gagosz, F. Gold(I)-Catalyzed Rearrangement of Propargyl Benzyl Ethers: A Practical Method for the Generation and in Situ Transformation of Substituted Allenes. *J. Am. Chem. Soc.* **2010**, 132, 7294–7296.
- 8- For Au(I)-catalyzed advancements developed by Toste and co-workers see: (a) Wu, H.; Zi, W.; Li, G.; Lu, H.; Toste, F. D. Gold(I)-Catalyzed Desymmetrization of 1,4-Dienes by an Enantioselective Tandem Alkoxylation/Claissen Rearrangement. *Angew. Chem. Int. Ed.* **2015**, 54, 8529–8532. (b) Zi, W.; Wu, H.; Toste, F. D. Gold(I)-Catalyzed Dearomative Rautenstrauch Rearrangement: Enantioselective Access to Cyclopenta[b]indoles. *J. Am. Chem. Soc.* **2015**, 137, 3225–3228. (c) Zi, W.; Toste, F. D. Gold(I)-Catalyzed Enantioselective Carboalkoxylation of Alkynes. *J. Am. Chem. Soc.* **2013**, 135, 12600–12603. (d) Wang, Y.-M.; Kuzniewski, C. N.; Rauniyar, V.; Hoong, C.; Toste, F. D. Chiral (Acyclic Diaminocarbene)Gold(I)-Catalyzed Dynamic Kinetic Asymmetric Transformation of Propargyl Esters. *J. Am. Chem. Soc.* **2011**, 133, 12972–12975. (e) Uemura, M.; Watson, I. D. G.; Katsukawa, M.; Toste, F. D. Gold(I)-Catalyzed Enantioselective Synthesis of Benzopyrans via Rearrangement of Allylic Oxonium Intermediates. *J. Am. Chem. Soc.* **2009**, 131, 3464–3465. (f) Shapiro, N. D.; Shi, Y.; Toste, F. D. Gold-Catalyzed [3 + 3]-Annulation of Azomethine Imines with Propargyl Esters. *J. Am. Chem. Soc.* **2009**, 131, 11654–11655. (f) Zhao, J.; Hughes, C. O.; Toste, F. D. Synthesis of Aromatic Ketones by a Transition Metal-Catalyzed Tandem Sequence. *J. Am. Chem. Soc.* **2006**, 128, 7436–7437. (g) Dube, P.; Toste, F. D. Synthesis of Indenyl Ethers by Gold(I)-Catalyzed Intramolecular Carboalkoxylation of Alkynes. *J. Am. Chem. Soc.* **2006**, 128, 12062–12063.
- 9- For Pt- and Pd-catalyzed cyclization methods see: (a) Nakamura, I.; Mizushima, Y.; Gridnev, I. D.; Yamamoto, Y. Stepwise Delivery of Two Methoxy Groups of Arylaldehyde Acetals across the Phenyl

- Ring. Vacant Site-Controlled Palladium Catalysis. *J. Am. Chem. Soc.* **2005**, *127*, 9844–9847. (b) Nakamura, I.; Mizushima, Y.; Yamamoto, Y. Synthesis of 2,3-Disubstituted Benzofurans by Platinum–Olefin-Catalyzed Carboalkoxylation of o-Alkynylphenyl Acetals. *J. Am. Chem. Soc.* **2005**, *127*, 15022–15023. (c) Nakamura, I.; Bajracharya, G. B.; Wu, H.; Oishi, K.; Mizushima, Y.; Gridnev, I. D.; Yamamoto, Y. Catalytic Cyclization of o-Alkynylbenzaldehyde Acetals and Thioacetals. Unprecedented Activation of the Platinum Catalyst by Olefins. Scope and Mechanism of the Reaction. *J. Am. Chem. Soc.* **2004**, *126*, 15423–15430.
- 10- For use of a 1,5-H shift in construction of carbocycle see: (a) Ikeuchi, T.; Inuki, S.; Oishi, S.; Ohno, H. Gold(I)-Catalyzed Cascade Cyclization Reactions of Allenynes for the Synthesis of Fused Cyclopropanes and Acenaphthenes. *Angew. Chem., Int. Ed.* **2019**, *58*, 7792–7796. (b) Nahide, P. D.; Jimenez-Halla, J. O. C.; Wrobel, K.; Solorio-Alvarado, C. R.; Alvarado, R. O.; Yahuaca-Juarez, B. Gold(I)catalysed high-yielding synthesis of indenenes by direct Csp³–H bond activation. *Org. Biomol. Chem.* **2018**, *16*, 7330–7335. (c) Zheng, Z.; Zhang, L. C–H insertions in oxidative gold catalysis: synthesis of polycyclic 2H-pyran-3(6H)-ones via a relay strategy. *Org. Chem. Front.* **2015**, *2*, 1556–1560. (d) Zhang, F.; Das, S.; Walkinshaw, A. J.; Casitas, A.; Taylor, M.; Suero, M. G.; Gaunt, M. J. Cu-Catalyzed Cascades to Carbocycles: Union of Diaryliodonium Salts with Alkenes Exploiting Remote Carbocations. *J. Am. Chem. Soc.* **2014**, *136*, 8851–8854. (e) Jin, T.; Himuro, M.; Yamamoto, Y. Brønsted Acid-Catalyzed Cascade Cycloisomerization of Enynes via Acetylene Cations and sp³-Hybridized C–H Bond Activation. *J. Am. Chem. Soc.* **2010**, *132*, 5590–5591. (f) Biermann, U.; Koch, R.; Metzger, J. O. Intramolecular Concerted Insertion of Vinyl Cations into C–H Bonds: Hydroalkylating Cyclization of Alkynes with Alkyl Chloroformates To Give Cyclopentanes. *Angew. Chem., Int. Ed.* **2006**, *45*, 3076–3079.
- 11- Yamada, T.; Park, K.; Tachikawa, T.; Fujii, A.; Rudolph, M.; Hashmi, A. S. K.; Sajiki, H. Gold-Catalyzed Cyclization of 2-Alkynylaldehyde Cyclic Acetals via Hydride Shift for the Synthesis of Indenone Derivatives. *Org. Lett.* **2020**, *22*, 1883–1888.
- 12- An initial version of this work was deposited in ChemRxiv on 07/31/2020, Reference 10.26434/chemrxiv.12745529.v1 (<https://chemrxiv.org/ndownloader/files/24120110>, <https://chemrxiv.org/ndownloader/files/24120119>).
- 13- (a) Duan, Y.; Liu, Y.; Bi, S.; Ling, B.; Jiang, Y.-Y.; Liu, P. Theoretical Study of Gold-Catalyzed Cyclization of 2-Alkynyl-N-propargylanilines and Rationalization of Kinetic Experimental Phenomena. *J. Org. Chem.* **2016**, *81*, 9381–9388. (b) Alcaide, B.; Almendros, P.; Fernández, I.; Martín-Montero, R.; Martínez-Peña, F.; Ruiz, M. P.; Torres, M. R. Gold-Catalyzed Reactivity Reversal of Indolizidinone-Tethered β -Amino Allenes Controlled by the Stereochemistry. *ACS Catal.* **2015**, *5*, 4842–4845.

- 14- Frisch, M. J.; Trucks, G. W.; Schlegel, H. B.; Scuseria, G. E.; Robb, M. A.; Cheeseman, J. R.; Scalmani, G.; Barone, V.; Mennucci, B.; Petersson, G. A.; Nakatsuji, H.; Caricato, M.; Li, X.; Hratchian, H. P.; Izmaylov, A. F.; Bloino, J.; Zheng, G.; Sonnenberg, J. L.; Hada, M.; Ehara, M.; Toyota, K.; Fukuda, R.; Hasegawa, J.; Ishida, M.; Nakajima, T.; Honda, Y.; Kitao, O.; Nakai, H.; Vreven, T.; Montgomery Jr., J. A.; Peralta, J. E.; Ogliaro, F.; Bearpark, M. J.; Heyd, J.; Brothers, E. N.; Kudin, K. N.; Staroverov, V. N.; Kobayashi, R.; Normand, J.; Raghavachari, K.; Rendell, A. P.; Burant, J. C.; Iyengar, S. S.; Tomasi, J.; Cossi, M.; Rega, N.; Millam, N. J.; Klene, M.; Knox, J. E.; Cross, J. B.; Bakken, V.; Adamo, C.; Jaramillo, J.; Gomperts, R.; Stratmann, R. E.; Yazyev, O.; Austin, A. J.; Cammi, R.; Pomelli, C.; Ochterski, J. W.; Martin, R. L.; Morokuma, K.; Zakrzewski, V. G.; Voth, G. A.; Salvador, P.; Dannenberg, J. J.; Dapprich, S.; Daniels, A. D.; Farkas, Ö.; Foresman, J. B.; Ortiz, J. V.; Cioslowski, J.; Fox, D. J. *Gaussian 09 Revision D.01*, Gaussian, Inc.: Wallingford, CT, USA, **2013**.
- 15- For suitability of B3LYP(a) Zhang, C.; Wang, G.; Zhan, L.; Yang, X.; Wang, J.; Wei, Y.; Xu, S.; Shi, M.; Zhang, J. Gold(I) or Gold(III) as Real Intermediate Species in Gold-Catalyzed Cycloaddition Reactions of Enynal/Enynone?. *ACS Catal.* **2020**, *10*, 6682–6690. (b) Noey, E. L.; Luo, Y.; Zhang, L.; Houk, K. N. Mechanism of Gold(I)-Catalyzed Rearrangements of Acetylenic Amine-N-Oxides: Computational Investigations Lead to a New Mechanism Confirmed by Experiment. *J. Am. Chem. Soc.* **2012**, *134*, 1078–1084. (c) Noey, E. L.; Wang, X.; Houk, K. N. Selective Gold(I)-Catalyzed Formation of Tetracyclic Indolines: A Single Transition Structure and Bifurcations Lead to Multiple Products. *J. Org. Chem.* **2011**, *76*, 3477–3483. (d) Liu, L.-P.; Malhotra, D.; Jin, Z.; Paton, R. S.; Houk, K. N.; Hammond, G. B. Gold-Catalyzed, Intramolecular, Oxygen-Transfer Reactions of 2-Alkynyl-1,5-diketones or 2-Alkynyl-5-ketoesters: Scope, Expansion, and Mechanistic Investigations on a New [4+2] Cycloaddition. *Chem. Eur. J.* **2011**, *17*, 10690–10699. (e) Liu, L.-P.; Malhotra, D.; Paton, R. S.; Houk, K. N.; Hammond, G. B., The [4+2], not [2+2], Mechanism Occurs in the Gold-Catalyzed Intramolecular Oxygen Transfer Reaction of 2-Alkynyl-1,5-Diketones. *Angew. Chem. Int. Ed.* **2010**, *49*, 9132–9135. (f) Cheong, P. H.-Y.; Morganelli, P.; Luzung, M. R.; Houk, K. N.; Toste, F. D. Gold-Catalyzed Cycloisomerization of 1,5-Allenynes via Dual Activation of an Ene Reaction. *J. Am. Chemical Soc.* **2008**, *130*, 4517–4526. (g) Tirado-Rives, J.; Jorgensen, W. L. Performance of B3LYP Density Functional Methods for a Large Set of Organic Molecules. *J. Chem. Theory Comput.* **2008**, *4*, 297–306.
- 16- Hay, P. J.; Wadt, W. R. Ab initio effective core potentials for molecular calculations. Potentials for the transition metal atoms Sc to Hg. *J. Chem. Phys.* **1985**, *82*, 270–283. (b) Wadt, W. R.; Hay, P. J. Ab initio effective core potentials for molecular calculations. Potentials for main group elements Na to Bi. *J. Chem. Phys.* **1985**, *82*, 284–298. (c) Hay, P. J.; Wadt, W. R. Ab initio effective core potentials for

- molecular calculations. Potentials for K to Au including the outermost core orbitals. *J. Chem. Phys.* **1985**, *82*, 299–310.
- 17- Schlegel, H. B. Optimization of equilibrium geometries and transition structures. *J. Comput. Chem.* **1982**, *3*, 214–218. (b) Li, X.; Frisch, M. J. Energy-Represented Direct Inversion in the Iterative Subspace within a Hybrid Geometry Optimization Method. *J. Chem. Theory Comput.* **2006**, *2*, 835–839.
- 18- Weigend, F.; Ahlrichs, R. Balanced basis sets of split valence, triple zeta valence and quadruple zeta valence quality for H to Rn: Design and assessment of accuracy. *Phys. Chem. Chem. Phys.* **2005**, *7*, 3297–3305.
- 19- Grimme, S.; Antony, J.; Ehrlich, S.; Krieg, H. A consistent and accurate ab initio parametrization of density functional dispersion correction (DFT-D) for the 94 elements H-Pu. *J. Chem. Phys.* **2010**, *132*, 154104.
- 20- Marenich, A. V.; Cramer, C. J.; Truhlar, D. G. Universal Solvation Model Based on Solute Electron Density and on a Continuum Model of the Solvent Defined by the Bulk Dielectric Constant and Atomic Surface Tensions. *J. Phys. Chem. B* **2009**, *113*, 6378–6396.
- 21- Hratchian, H. P.; Schlegel, H. B. Accurate reaction paths using a Hessian based predictor-corrector integrator. *J. Chem. Phys.* **2004**, *120*, 9918–9924. (b) Collins, M. A. Molecular potential-energy surfaces for chemical reaction dynamics. *Theor. Chem. Acc.* **2002**, *108*, 313–324. (c) Fukui, K. The path of chemical reactions - the IRC approach. *Acc. Chem. Res.* **1981**, *14*, 363–368.
- 22- Legault, C. Y. CYLview, 1.0b; Université de Sherbrooke: Canada, **2009**; <http://www.cylview.org>.
- 23- Johnson, E. R.; Keinan, S.; Mori-Sánchez, P.; Contreras-García, J.; Cohen, A. J.; Yang, W. Revealing Noncovalent Interactions. *J. Am. Chem. Soc.* **2010**, *132*, 6498–6506.
- 24- Lu, T.; Chen, F. Multiwfn: A multifunctional wavefunction analyzer. *J. Comput. Chem.* **2012**, *33*, 580–592.
- 25- Humphrey, W.; Dalke, A.; Schulten, K. VMD - Visual Molecular Dynamics. *J. Molec. Graphics*, **1996**, *14*, 33–38.